Supporting Online Material for

Electromechanical Resonators from Graphene Sheets

J. Scott Bunch, Arend M. van der Zande, Scott S. Verbridge, Ian W. Frank,
David M. Tanenbaum, Jeevak M. Parpia, Harold G. Craighead, Paul L. McEuen*

*To whom correspondence should be addressed. E-mail: mceuen@ccmr.cornell.edu

Published 26 January 2007, *Science* **315**, 490 (2007)
DOI: 10.1126/science.1136836

This PDF file includes:

Supporting Online Material.

Materials and Methods

Suspended graphene sheets are fabricated using a peeling process. A freshly cleaved piece of Kish graphite (Toshiba Ceramics) is rubbed onto a silicon wafer with 260 - 330 nm (280 nm ideal) of thermally grown SiO_2. Trenches with a depth of 260 - 500 nm and widths and lengths of 0.5 – 10 μm are defined on the SiO_2 by dry RF plasma etching. Electrodes are defined by photolithography and consist of 5 nm of Cr and 30 nm Au. The graphene sheets peel off on the edges of the large trenches and electrodes and are suspended over nearby small trenches.

The optical drive is done using a 432 nm diode laser which is intensity modulated at a frequency defined by the network analyzer and focused on the suspended graphene (Fig. S1). The suspended graphene sheet and the silicon back plane form an interferometer through which vibrations are detected by looking at variations in the intensity of the reflected light from a second 632.8 nm He-Ne laser focused on the resonators (*1*). Electrical drive is accomplished by combining a time varying RF voltage from the RF output of an Agilent E4402B Spectrum Analyzer and a DC voltage from a Yukogawa 7651 DC source.

All non-contact mode AFM images are taken using a Dimension 3100 operating in ambient conditions using silicon cantilevers with resonant frequencies of 250 – 350 kHz. Raman spectroscopy is performed using a Renishaw InVia Raman microscope. Light with a wavelength of 488 nm is focused on the resonator using a 50x objective and each Raman trace is taken with a 1 - 5 second integration time. The sample sits on a piezoelectric stage which is scanned to take a Raman spectrum at specific points along the graphene sheet.

Supplementary Material

Electrostatic actuation and tuning of the resonant frequency

Data for electrical drive on resonance for the 1.5 nm thick graphene sheet in Fig. 1D are shown in Fig. S2. The amplitude and frequency of the fundamental mode as well as the higher mode increase linearly with V_g^{DC} at a fixed δV_g as expected from equation (1) in the main text (Fig. S2 C). Also shown is a plot of the resonant frequency vs. V_g^{DC} at a fixed δV_g for both modes (Fig. S2 D). In this case, the higher mode increases in frequency with V_g^{DC} while the fundamental mode is unchanged. Most of the modes measured in different resonators exhibited either no tuning or positive tuning in which the frequency increased with V_g^{DC}. A few of the resonators displayed negative tuning where the frequency decreased with increasing V_g^{DC}. The fundamental mode for the resonator in Fig. 4 displayed such negative tuning (Fig. S3 B). Resonators with frequencies lower than expected (presumably with slack) such as the one in Fig 4 and S3, decrease in frequency with capacitive force. Resonators with tension (the majority) either show no tuning or an increase in frequency with capacitive force. The different kinds of tuning have previously been observed in other NEMS devices and attributed to spring constant softening due to the electrostatic attraction to the gate, increasing tension from stretching, and a transition from bending to catenary regime (*2, 3*).

Young's Modulus and Tension

The Young's modulus remains a useful concept for atomic scale devices provided the right effective thickness is used (*4*). There is extensive theoretical work on the mechanical properties of carbon nanotubes which are rolled up graphene sheets, and a Young's modulus for these nanostructures is commonly used. However, there is a significant variation in the literature of both the accepted and measured values of the Young's modulus (*4*). Determining inferred tension from the Young's modulus is misleading for thick resonators, because any error in the Young's modulus results in a large error in the inferred tension. However, it still is accurate to deduce the tension in the thinner resonators since many of these are in a high tension limit.

The tension in resonators with $t < 7$ nm was inferred to be 10^{-8} to 10^{-6} N. The single layer resonator in the text has a tension of 10 nN and strain of 10^{-3} %. This is reasonable considering the large van der Waals attraction between the graphene and silicon oxide. Our group has strained carbon nanotubes lying on an oxide surface up to 2 percent, and the van der Waals force remains sufficient to hold the nanotube in place. The Lieber and Park group at Harvard have reported that the van der Waals force is sufficiently strong to hold strains as high as 10 percent for a nanotube on oxide (*5*). So far we are unable to control the tension for the resonator since it is a random process affected by how the graphene happens to peel.

Quality Factor

There was no striking dependence of Q on thickness, frequency, or mode number in our graphene resonators. Upon cooling, the Q increased for most of the devices, but this was accompanied by noise in the frequency position of the resonant frequency peak, making a systematic study difficult.

No clear dependence of quality factor on resonator thickness was observed. This suggests that the dominant dissipation mechanism is different than that of standard silicon NEMS. Since the structure and quality factor of graphene resonators is similar to carbon nanotube resonators, it is possible that the dissipation mechanism is similar. However, there is currently no clear understanding of the dissipation mechanism in carbon nanotube resonators. An extrinsic mechanism such as clamping loss or fluctuating charge noise may dominate dissipation in graphene resonators.

Using thermal motion to calculate the resonator amplitude

To detect thermal vibrations, both large thermal amplitude (low spring constant) and large reflectivity (high optical signal) from the graphene is required. This was only the case for a few of the resonators studied.

After determining the resonance frequency of a particular resonator we turn off the drive and measure the fluctuations. The voltage noise power spectrum $S_v^f = V^2/B$, where V is the voltage output of the photodiode and B is the resolution bandwidth. S_V^f has a contribution from a constant background electrical noise in the system, $S^f_{electrical}$, and a contribution from the thermal mechanical oscillation peak, S_x^f. $S^f_{electrical}$ and S_x^f are incoherent noise sources so their contributions to the voltage power add linearly such that $S_v^f = S^f_{electrical} + \alpha\, S_x^f$, where α is a constant scaling factor relating resonator displacement with changes in the measured photodetector voltage.

The thermal oscillation of a resonator is expected to have a spectral density given by:

$$S_x^f = \frac{2k_B T f_0^3}{\pi \kappa_{\text{eff}} Q} \text{ x } \frac{1}{(f_0^2 - f^2)^2 + (f\, f_0/Q)^2} \qquad \text{(S1)}$$

where the total thermal motion of a resonance peak must obey the equipartion theorem.

$$x_{th}^2 = \int_0^\infty S_x^f \, df = \frac{k_B T}{\kappa_{eff}} \qquad \text{(S2)}$$

Fitting the voltage power spectral density S_v^f to the theoretical distribution S_x^f, we determine the scaling factor α.

The amplitude of a driven resonance, x_{driven}, is related to the measured voltage signal, $V_{driven,}$ by:

$$x^2_{driven} = (V^2_{driven} - V^2_{background})/\alpha \qquad \text{(S3)}$$

Once again, $V_{background}$ is the constant offset due to the background electrical noise. It is important to note that the scaling factor is dependent on the device measured as well as the precise optical conditions such as laser focus and spot location. Any changes to these parameters require a recalibration of the scaling factor.

Mass detection sensitivity

The low effective mass coupled with high surface area makes graphene resonators ideal candidates for mass sensing. The minimum detectable mass for a resonator is:

$$\delta M \approx 2\frac{m_{eff}}{Q} 10^{-DR/20} \qquad \text{(S4)}$$

where the dynamic range, *DR*, is the decibel measure of the ratio between the amplitude of onset of non-linearity to the noise floor (*6*). For the resonator shown in Fig. 4, the dynamic range is ~ 60 dB, giving a room temperature mass sensitivity of ~ 450 zeptograms. This is comparable in sensitivity to current state of the art room temperature NEMS (*7*). Even though the mass is much lower than standard NEMS due to the small thickness of graphene, the quality factor at room temperature is lower by a similar amount. This suggests that mass sensing with graphene NEMS would be greatly enhanced by improving the quality factor.

Supplementary Figures

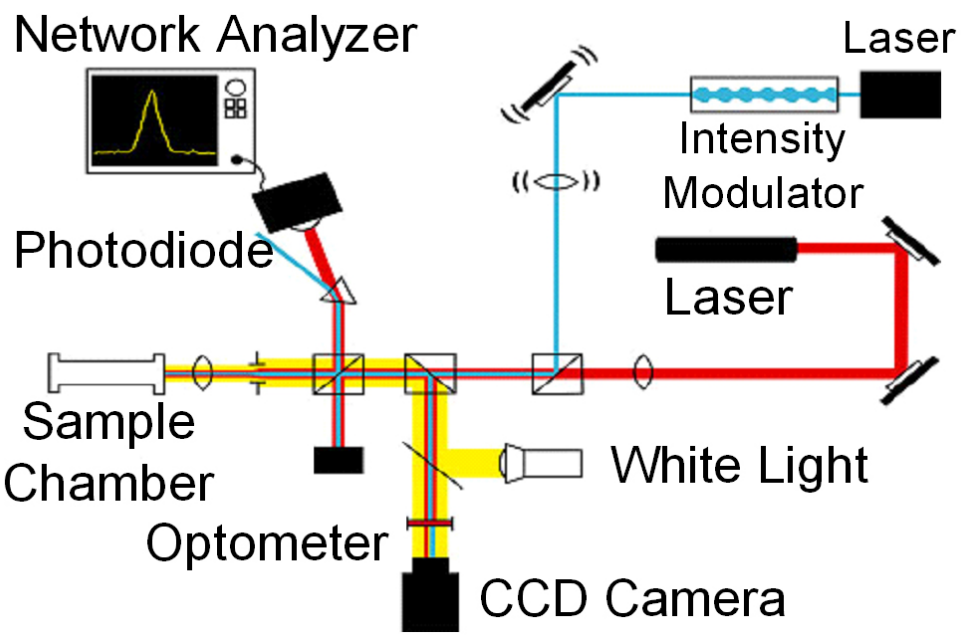

Figure S1. Schematic of the experimental setup used to actuate and detect vibrations.

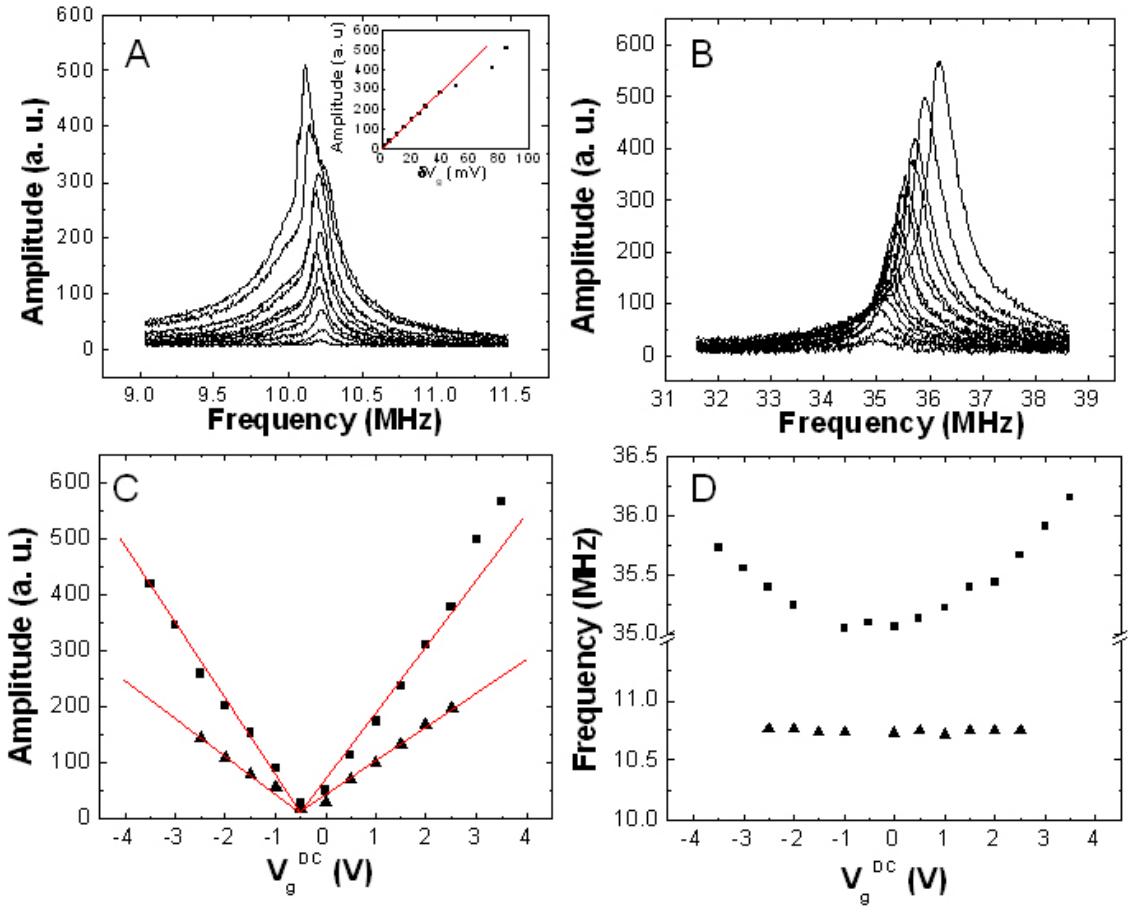

Figure S2 (A) Amplitude versus frequency for the fundamental mode from the resonator shown in Figure 1(D) taken using electrical drive with V_g^{DC} = 2 V and increasing δV_g. (inset) The amplitude on resonance as a function of δV_g. (B) Amplitude versus frequency of a higher mode from the resonator shown in Figure 1(B) taken using electrical drive with δV_g = 15 mV and increasing V_g^{DC}. (C) Amplitude of oscillation versus V_g^{DC} at δV_g = 15 mV for both the 10 MHz mode (▲) and 35 MHz mode (■). (D) Frequency versus V_g^{DC} at δV_g = 15 mV for both the 10 MHz mode (▲) and 35 MHz mode (■).

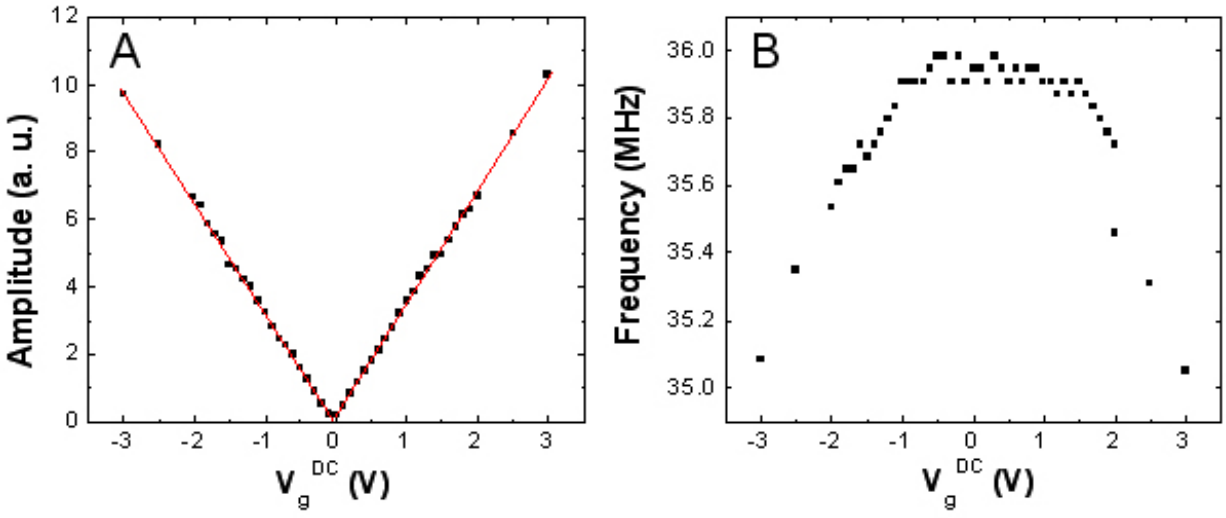

Figure S3 (A) Amplitude of oscillation versus V_g^{DC} at δV_g = 50 mV for the fundamental mode shown in Fig. 4. (B) The frequency at maximum amplitude versus V_g^{DC} at δV_g = 50 mV for the fundamental mode shown in Fig. 4.

Supplementary References

1. B. Ilic, S. Krylov, K. Aubin, R. Reichenbach, H. G. Craighead, *Appl. Phys. Lett.* **86**, 193114 (May, 2005).
2. I. Kozinsky, H. W. C. Postma, I. Bargatin, M. L. Roukes, *Appl. Phys. Lett.* **88**, 253101 (2006).
3. V. Sazonova *et al.*, *Nature* **431**, 284 (2004).
4. D. Qian, G. J. Wagner, W. K. Liu, M.-F. Yu, R. S. Ruoff, *Applied Mechanics Reviews* **55**, 495 (2002).
5. D. Bozovic *et al.*, *Phys. Rev. B* **67**, 033407 (2003).
6. K. L. Ekinci, M. L. Roukes, *Rev. Sci. Instrum.* **76**, 061101 (2005).
7. B. Ilic et al., *Journal of Applied Physics* **95**, 3694 (2004).